ELSEVIER

International Journal of Mass Spectrometry 190/191 (1999) 81–102

International Journal of Mass Spectrometry

Fundamental studies of ion injection and trapping of electrosprayed ions on a quadrupole ion trap

Scott T. Quarmby[1], Richard A. Yost*

Department of Chemistry, University of Florida, Gainesville, FL 32611-7200, USA

Received 6 July 1998; accepted 10 August 1998

Abstract

The quadrupole ion trap is a highly versatile and sensitive analytical mass spectrometer. Because of the advantages offered by the ion trap, there has been intense interest in coupling it to ionization techniques such as electrospray which form ions externally to the ion trap. In this work, simulation and experiment were employed to study the injection of electrosprayed ions into the quadrupole ion trap in a Finnigan MAT LCQ LC/MS^n mass spectrometer. SIMION v6.0 was chosen for the simulation studies because it allowed the actual ion trap electrode geometry including endcap holes to be simulated. The endcap holes weaken the rf trapping field in the region near the holes; this distortion of the field is important when ions have large axial excursions as they do in ion injection. In addition, the field penetrates out the endcap holes and affects ions as they approach the ion trap. The results of simulating ions started outside the ion trap agreed well with experimentally obtained ion injection data of the effect of q_z during injection. From these simulations, a model for the process by which injected ions are trapped was developed. Injected ions can be trapped even with the modest helium buffer gas pressures commonly used (≈1 mTorr) because ions naturally oscillate for long times (and therefore distances) at certain q_z values and initial rf phases. This allows enough collisions to occur to damp the ions' excess kinetic energy. (Int J Mass Spectrom 190/191 (1999) 81–102) © 1999 Elsevier Science B.V.

Keywords: Quadrupole ion trap; Ion injection; Electrospray; Simulation

1. Introduction

The quadrupole ion trap first described by Paul and Steinwedel [1] has evolved from an ion storage device into a highly successful analytical mass spectrometer. Commercially, the ion trap has primarily been used with electron ionization and chemical ionization performed within the ion trap. Because of the advantages offered by the ion trap, there has been significant interest in coupling it to ionization techniques such as electrospray; however, electrospray and many other ionization techniques require ions to be formed externally and then injected into the ion trap. As a result, many studies of ion injection have appeared [2–4] and new techniques have been developed for increasing the efficiency that injected ions are trapped with [5–10].

It has long been recognized that ions injected into an ion trap, with a constant rf voltage applied to the ring electrode, cannot be trapped indefinitely because

* Corresponding author. E-mail: ryost@chem.ufl.edu

[1]Present address: Finnigan Corporation, 2215 Grand Avenue Parkway, Austin, TX 78728.

Dedicated to J.F.J. Todd and R.E. March in recognition of their original contributions to quadrupole ion trap mass spectrometry.

PII S1387-3806(98)14268-9

of the excess kinetic energy which allowed them to enter the ion trap in the first place [11]. Some method of removing excess kinetic energy is necessary, with collisional damping with a buffer gas being the most common [2]. Trapping ions from continuous ionization sources such as electrospray has been shown to be relatively inefficient, with less than 5% of the total ions being trapped [10,12]. This low efficiency was explained by computer simulations which showed that ions were only trapped over a small range of rf phases [13,14]. However, the process by which injected ions are trapped is still not well understood. In this work, computer simulations were used to model the injection of ions produced in an electrospray ionization source into the ion trap in a Finnigan MAT LCQ LC/MS^n mass spectrometer. The results of the simulations were compared with experimental ion injection data; based upon these results, a model for the process of how injected ions are trapped is presented.

The Finnigan MAT ion trap uses a "stretched" electrode geometry different from the ideal quadrupole field [15,16]; therefore, any simulation must include effects from higher-order fields such as hexapole and octopole in addition to the main quadrupole trapping field [4,17]. However, a potential equation which includes higher-order field terms cannot be represented in closed form and therefore cannot be solved implicitly. As a result, a numerical integration technique such as finite-element analysis or finite-difference analysis is necessary to calculate the potential within the ion trap. Several groups have developed computer simulations of ion trajectories that can solve these potential equations which include higher-order fields. The use of finite-element analysis to study quadrupole ion traps was first reported in 1989 [18]. The nonlinear ion trap simulation of Franzen and co-workers has been used to simulate ion traps with different percentages of higher-order fields [19,20]. The nonlinear ion trap simulation was also used to simulate ion injection (with ions started at the endcap boundary) including the effect of higher buffer gas pressure [8]. March and co-workers developed the field interpolation method (FIM) to simulate ion traps which contain higher-order fields and employ monopole and dipole resonant excitation [21,22]. FIM can simulate any electrode geometry given the equations for the surfaces. The ion trap simulation program, ITSIM, developed by Cooks and co-workers is a multiparticle simulation which calculates the potentials in the ion trap by the multipole expansion of the Legendre polynomials [23–25]. This technique also allows the simulation of ion trap geometries which include percentages of higher-order fields. It has been used to study many different modes of ion trap operation including ion injection [9].

All of these simulations allow higher-order fields (e.g. hexapole and octopole) to be included as percentages of the main quadrupole field. However, the only one of these simulation programs which can model endcap holes is the finite-element analysis program developed by Lunney and co-workers [18]. Holes in the endcap electrodes are necessary for ions to enter the ion trap and then exit to be detected. Only a simulation that allows the potential in the ion trap to be calculated from any arbitrary electrode surface geometry (not just continuous equations) can accurately simulate the effects of endcap holes. The endcap holes distort the rf field in a relatively complex manner which cannot be modeled simply by superimposed higher-order fields [26]. For many simulations, the effect of the endcap holes may be negligible; however, when ions are injected into the ion trap and therefore have large trajectories where the ions approach the endcap holes, the holes may be very important. In addition, the effect of the rf field as ions approach the ion trap can only be studied if endcap holes are included in the simulation.

To model the effect of endcap holes, a simulation is required which models the actual electrode geometry, rather than representing the electrodes by equations. SIMION v6.0 (Idaho National Engineering Laboratory, Idaho Falls, ID) allows the actual electrodes to be simply gridded point by point. The potential at each point is then calculated using an over-relaxation finite difference technique; these potentials are then used to calculate the electric field gradient and the force on the ion. The position and velocity of the ion at the next time step is calculated using a fourth-order Runge–Kutta numerical integration.

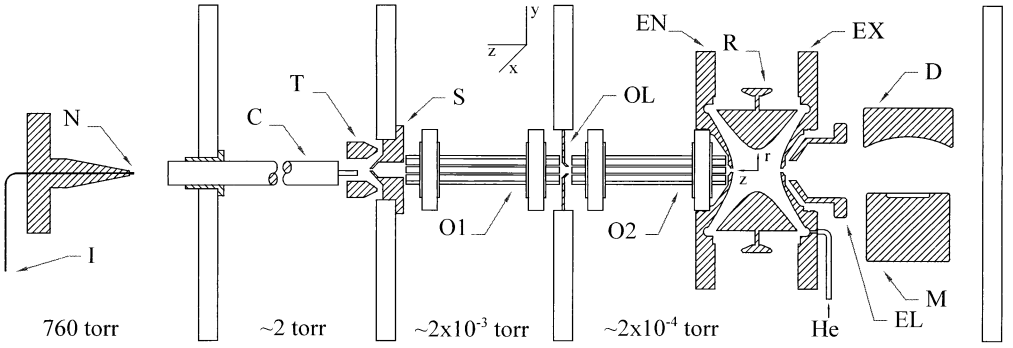

Fig. 1. Schematic of Finnigan MAT LCQ LC/MS^n quadrupole ion trap mass spectrometer equipped with electrospray ionization source. I—sample inlet; N—electrospray needle; C—heated capillary; T—tube lens; S—skimmer cone; O1—first octopole ion guide; OL—inter-octopole lens; O2—second octopole ion guide; EN—entrance endcap; R—ring electrode; EX—exit endcap; EL—exit lens; D—conversion dynode; M—electron multiplier. The approximate pressure in each region of the system is shown as well as the gas inlet (He) which supplies the helium buffer gas directly into the ion trap. Because of the pumping conductance out of the ion trap, the helium pressure in the ion trap is approximately 10 to 20 times higher than that in the chamber.

In this article, we show the first large scale computer simulations of ion injection into a quadrupole ion trap. A series of simulations are shown with and without endcap holes and an argument is presented for why it is critical to include the endcap holes in any simulations of ion injection. The simulations were run with enough ions started under enough different initial conditions to allow comparison with experimental ion injection data. The good agreement between the simulation results and the experimental data allowed the development of a model of how injected ions are trapped.

2. Experimental

2.1. Ion motion in a quadrupole field

The theory of the quadrupole ion trap has been reviewed extensively [4,27]. Basically, a potential difference consisting of a dc voltage, U, and an ac voltage of amplitude (zero-to-peak), V, and angular frequency, Ω, is applied between the ring electrode and the two endcap electrodes. The radius of the ring electrode is defined as r_0 and the distance from the center of the ion trap to the closest point on the endcap electrodes is defined as z_0. With the most common choice of hyperbolic surface geometry for the ring and endcap electrodes, a pure quadrupole field is created when $r_0^2 = 2z_0^2$ [28]. The motion of an ion of mass-to-charge ratio, m/e, in the quadrupole ion trap is governed by the Mathieu equation which contains the reduced parameters a and q given by the following equations [27]:

$$a_z = -2a_r = \frac{-16eU}{m\Omega^2(r_0^2 + 2z_0^2)} \quad (1)$$

$$q_z = -2q_r = \frac{8eV}{m\Omega^2(r_0^2 + 2z_0^2)} \quad (2)$$

In all of this work, the dc voltage, U, applied to the ring electrode was 0 V making $a_z = 0$.

2.2. Ion injection experiments on LCQ

All experiments were performed on a modified Finnigan MAT LCQ LC/MS^n quadrupole ion trap mass spectrometer equipped with an electrospray ionization (ESI) source. As with previous Finnigan MAT ion trap instruments, the LCQ does not use the ideal electrode spacing, $r_0^2 = 2z_0^2$. The LCQ uses $r_0 = 7.07$ mm and $z_0 = 7.85$ mm, instead of the theoretical $z_0 = 5.00$ mm (previous Finnigan MAT ion traps had $r_0 = 10.00$ mm and $z_0 = 7.83$ mm) [29]. The instrument employed an angular frequency,

$\Omega/2\pi$, of 760 kHz and achieved an m/z range of 1850 Da. A schematic of the LCQ is shown in Fig. 1. Note that in contrast to previous Finnigan MAT ion traps, the LCQ has a single hole in each endcap electrode to allow ions to enter and exit. Ions are formed by ESI at atmospheric pressure and collected by a heated metal capillary. Ions exiting the heated capillary are focused by a tube lens and then passed through a skimmer cone into a 2 in. long rf-only octopole ion guide. After a lens, which serves as a conductance limit, a second octopole transports ions into the ion trap.

For the ion injection experiments, L-serine, MW = 105.1 Da (Sigma Chemical Co., St. Louis, MO) and Ultramark 1621 (PCR, Gainesville, FL) were used. L-serine was dissolved in 49.5:49.5:1 methanol: water: acetic acid. A 5 nmol/μL concentration was infused at 3 μL/min and electrosprayed. Ultramark 1621 was dissolved in 49.7:24.7:24.7:1.0 acetonitrile: methanol: water: acetic acid. A 0.1% concentration was infused at 3 μL/min and electrosprayed. Custom instrument control software was used to vary the injection q_z and to record the resulting ion signal.

2.3. Ion injection simulations using SIMION v6.0

SIMION v6.0 was used to model ion injection on the LCQ including the effects of the endcap holes on ion trajectories. The LCQ electrodes were input into SIMION on an 800 by 800 grid; this was the largest workspace possible for the 120 MHz Pentium computer with 32 Mbytes of RAM that was used. Portions of the exit lens and the second octopole were also gridded. In order to maintain cylindrical symmetry and save memory, the octopole was modeled as a cylindrical tube lens. The electrodes were refined using an iteration limit of 50 000, an over-relaxation factor of 0.90, a historical memory factor of 0.70, and a convergence objective of 5×10^{-6}. The default computational quality of 2 was used unless otherwise noted. A user program was written which allowed rf and dc voltages to be applied to the ring electrode.

A one-dimensional Monte Carlo hard-sphere collision model was incorporated into the user program to simulate the random collisions with helium buffer gas. In this collision model, the distance an ion traveled before colliding, l, was calculated using the following equation [30]:

$$l = -\frac{\ln(1-\zeta)}{\sigma n} \tag{3}$$

where ζ is a random number between 0 and 1, σ is the collision cross section, and n is the number density of the buffer gas. Once the ion had traveled this randomly determined distance, it was assumed to have a collision. In this one-dimensional model, the ion's kinetic energy was reduced using the following equation:

$$E' = E\,\frac{m^2 + m_{\mathrm{He}}^2}{(m + m_{\mathrm{He}})^2} \tag{4}$$

where E and E' are the kinetic energies before and after the collision, respectively, m is the mass of the ion, and m_{He} is the mass of a helium atom. The random distance to the next collision was then calculated and the process repeated. By reseeding the random number generator, a different collision sequence is produced. Using different random number generator seeds for a series of injected ions, statistical information was obtained on the percentage of ions which were trapped. In these studies, ten ions were injected at each set of conditions with different random number generator seeds. Studies with larger populations did not yield significantly different results.

Collisions were assumed to occur at all spatial locations including outside the ion trap (note that in the LCQ ion trap, the pressure of helium inside the ion trap is approximately ten times higher than outside). Unless otherwise noted, a simulated pressure of 1.5 mTorr helium ($n = 4.8 \times 10^{13}$ cm^{-3}) was used. The collision cross section, σ, of the ion provides some measure of the size of the ion. A few papers have been published giving values for collision cross sections of ions; from these a value of 50 Å^2 was chosen for m/z 100 ions colliding with helium atoms [31–34]. For simulations of other m/z ions, the following equation was used to approximate the collision cross section of any m/z ion relative to an m/z 100

ion. The equation is based on the assumptions that the ions are spherical and of equal density.

$$\sigma = 50 \left(\frac{m}{100} \right)^{2/3} \quad (5)$$

where m is the mass of the ion whose collision cross section is to be calculated. For example, an m/z 1522 ion would have a collision cross section of 307 Å^2 or approximately six times that of an m/z 100 ion. This value was rounded off to 300 Å^2 and used for all simulations of m/z 1522 ions.

2.4. Ion injection simulations of m/z 100 ions

The parameters which were predicted to have the largest influence on ion injection were the q_z during injection and the initial rf phase. The initial rf phase, ϕ_{rf}, was defined by the relationship $V \sin(\Omega t + \phi_{rf})$. For this work, ϕ_{rf} was varied between $-180°$ and $+179°$. When ions were started at a ϕ_{rf} of $-180°$ or 0°, the voltage applied to the ring is initially 0 V; at $\phi_{rf} = 90°$, the voltage is at a maximum ($+V$), and at $\phi_{rf} = -90°$ the voltage is at a minimum ($-V$). For all experiments, ten ions were individually injected at each set of experimental parameters with different random number generator seeds (and therefore collision sequences) to determine the percentage of ions trapped under those conditions. An ion was considered to be trapped if it underwent a stable trajectory for at least 400 μs without being lost to an electrode surface or an endcap hole. Monitoring ions for longer times increased the simulation time but did not produce significantly different results.

2.4.1. Effect of endcap holes on ion injection

To determine the effect of endcap holes, two different SIMION electrode grids were refined. The first grid included one hole (0.060 in. diameter) in each endcap electrode, while the second did not have holes in either endcap. For the first set of ion injection experiments, ions were started at the inner plane of the entrance endcap electrode with an initial position $z_{init} = z_0 = 7.85$ mm, $x_{init} = 0$ mm, and $y_{init} = 0$ mm (see Fig. 1). The ions were given an initial kinetic energy, E_0, at an angle, Θ, measured from the z axis. To determine an appropriate initial kinetic energy, stopping potentials were measured experimentally using m/z 106.1 ($[M + H]^+$ ion of L-serine). For these measurements, the dc offset on the second octopole, V_{O2}, was increased in steps of 0.125 V until the ion signal was attenuated by approximately three orders of magnitude. During these experiments the dc offset on the first octopole, V_{O1}, was -3 V and the dc offset on the ion trap, V_{trapdc}, was -10 V. The ion signal for m/z 106.1 was recorded for V_{O2} between -6 and $+2$ V. The maximum of the first derivative of these data gave the mean stopping potential, V_{O2stop}. This value was -2.88 ± 0.13 V for m/z 106.1. The normal operating V_{O2} is -6.5 V, meaning ions enter the second octopole with a kinetic energy of $z(V_{O2stop} - V_{O2}) = 3.62 \pm 0.13$ eV for singly charged ions. As ions enter the ion trap they gain another $z(V_{O2} - V_{trap}) = 3.5$ eV, resulting in an ion beam with a mean kinetic energy of approximately 7 eV. For the following simulations, an initial kinetic energy, E_0, of 7 eV was used.

Experimentally, ions of m/z 100 were predicted to be efficiently trapped when injected at a q_z of approximately 0.25 for an ion trap offset, V_{trapdc}, of -10 V. Using this q_z during injection, ten ions were injected at each initial rf phase between $-180°$ and 179° in 1° increments to determine the percentage of ions trapped at each phase.

2.4.2. Ions injected from outside ion trap

To determine what effect, if any, the rf trapping field had on ions which enter from outside the ion trap, ions were next started outside the ion trap and injected through the endcap hole. In these simulations, ions were started with a $z_{init} = 19$ mm from the center of the ion trap to model ions traveling from the octopole toward the entrance endcap. The octopole, modeled as a cylindrical tube lens, was held at a potential of -6.5 V, the same as the experimental V_{O2}. In these simulations, ions were started with an E_0 equal to the experimental kinetic energy of ions in the second octopole, $E_0 = 3.5$ eV, so that they accelerated to 7 eV as they entered the ion trap which was held at a dc offset of -10 V. Ions were injected

at different combinations of q_z and initial rf phase to map the effect of these parameters on trapping efficiency. Since ions could not be started with very large angles from the z axis, Θ, and still make it successfully through the endcap hole, ions were started with various x_{init} offsets with $y_{init} = 0$ mm. By again starting ions at each rf phase and calculating the percentage of ions trapped over all rf phases, it was found that ions started at an x_{init} of 0.2 mm were trapped most efficiently (data not shown). An x_{init} of 0.2 mm was used for all subsequent simulations; to put this value into perspective, the inscribed radius of the octopole rods is 2.79 mm. A large portion of the initial axial kinetic energy of the ions was lost due to collisions in the first octopole. Off-axis, or radial, kinetic energy will be damped at the same time. Considering this collisional cooling, ions should have trajectories close to the center of the second octopole.

2.5. Ion injection simulations of m/z 1522 ions

For comparison, ions of m/z 1522 were also simulated to determine the effect of a higher m/z.

2.5.1. Effect of endcap holes on ion injection

For the first set of ion injection experiments, ions were started at the inner plane of the entrance endcap electrode with an initial position $z_{init} = z_0 = 7.85$ mm, $x_{init} = 0$ mm, and $y_{init} = 0$ mm (see Fig. 1). The ions were given an initial kinetic energy, E_0, at an angle, Θ, measured from the z axis. As with the m/z 100 ions, an appropriate initial kinetic energy was determined using experimental stopping potential measurements. For m/z 1522, one of the $[M + H]^+$ ions of Ultramark 1621 was used. The average kinetic energy of m/z 1522 ions entering the ion trap was found to be 7.5 eV.

2.5.2. Ions injected from outside ion trap

Next, ions were started outside the ion trap and injected through the endcap hole. In these simulations, ions were started with a $z_{init} = 19$ mm from the center of the ion trap to model ions traveling from the octopole toward the entrance endcap. As with m/z 100, the octopole was held at a potential of −6.5 V. In these simulations, ions were started with an E_0 equal to the experimental kinetic energy of ions in the second octopole, $E_0 = 4.0$ eV, so that they accelerated to 7.5 eV as they entered the ion trap which was held at a dc offset of −10 V. An x_{init} of 0.2 mm was used for all simulations.

3. Results and discussion

3.1. Ion injection simulations of m/z 100 ions

3.1.1. Effect of endcap holes on ion injection

Ion injection simulations were performed for ions started at the inner plane of the entrance endcap. Two different SIMION electrode grids were used. The first grid included one endcap hole in each electrode, while the second did not have holes in either endcap. The parameters that were predicted to have the largest influence on ion injection were the q_z during injection and the initial rf phase; in addition, the effect of the injection angle, Θ, was also studied. Previous ion injection simulations have shown that larger injection angles produce more efficient trapping [14,35–38]. Ions of m/z 100 were injected at different initial angles, Θ, with $E_0 = 7$ eV, and a $q_z = 0.25$. Ten ions were injected at each rf phase between −180° and 179° in 1° increments to determine the percentage of ions trapped at each phase. A plot of the percentage of ions trapped at each rf phase is shown in Fig. 2(a) for $\Theta = 5°$. It was found that ions which were started at rf phases around 55° and −45° were successfully trapped; however, no ions were trapped at other rf phases. This partially explains the low trapping efficiency of externally produced ions from continuous ionization sources, since ions are only trapped if they arrive in the ion trap at a small range of rf phases.

Other injection angles (Θ = 0°, 5°, 10°, 15°, 20°, 30°, and 45°) were also studied. Based on these simulations, some general observations can be made. At an injection angle of 0°, ions that arrived at rf phases which allowed them to enter the ion trap tended to travel straight through and out the opposite endcap hole. Conversely, ions injected at angles of 20° and larger had significant amounts of radial

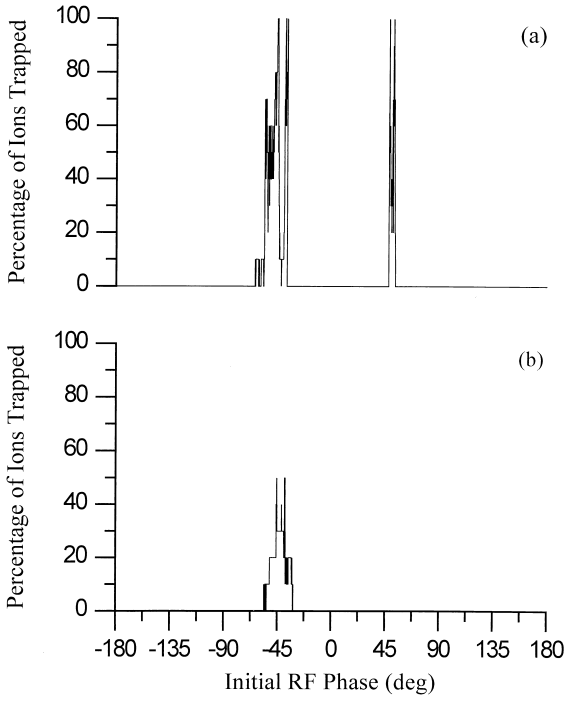

Fig. 2. Effect of endcap holes on the percentage of ions trapped as a function of initial rf phase. Ions of m/z 100 started at the inner plane of the entrance endcap ($z_{init} = z_0 = 7.85$ mm, $x_{init} = 0$ mm, and $y_{init} = 0$ mm) with $E_0 = 7$ eV and $\Theta = 5°$; simulated helium pressure of 1.5 mTorr; $q_z = 0.25$. Simulation (a) with and (b) without endcap holes.

kinetic energy and often hit the ring electrode. Ions with angles larger than 30° often had insufficient axial kinetic energy to penetrate more than 1 mm into the ion trap before being turned around into the endcap electrode. To compare the effect of different Θ angles quantitatively, the total number of ions trapped over all rf phases was summed and divided by the total number of ions injected over all rf phases, in this case (360 phases) $\times$ (10 ions/phase) = 3600 ions. At the most efficient angle, $\Theta = 5°$, 3.6% of the ions were trapped; thus, this injection angle was used for subsequent simulations.

The other point to note from Fig. 2(a) is that there are two ranges of rf phases for which efficient trapping of ions is observed. This is in contrast to previous simulations [8,9] which only predict trapping at the phase range around −45°. This discrepancy was puzzling at first, but close examination of the ion trajectories at these two sets of rf phases revealed that the endcap holes played a significant role in ion trapping. Since the distorted field caused by the endcap holes was not accounted for by previous simulations, this seemed like a probable explanation. To test this hypothesis, the simulation grids which omitted the endcap holes were used and the simulations repeated using the same conditions as in Fig. 2(a); the results are shown in Fig. 2(b). Without endcap holes, only one range of rf phases resulted in efficient trapping, as observed in previous simulations. Also, the efficiency with which ions are trapped at these phases is only about half as much without endcap holes as with endcap holes.

It was not clear if the extra range of efficient phases around 55° was just an artifact of the initial position of the ions in these simulations. At initial rf phases between 0° and 180°, the voltage on the ring is initially positive; ions are initially pushed back toward the endcap; without an endcap hole, they strike the endcap. When endcap holes were included in the model, the ions can sometimes back up into the entrance endcap hole without being lost until the voltage on the ring swings negative [5]. The simulations were repeated for ions started 0.5 mm inside the endcap electrode; the results are shown in Fig. 3(a) and (b). As before, ions were trapped over two ranges of rf phases when endcap holes were included and only one range of rf phases with no endcap holes. The rf phases which produced efficient trapping shifted to higher rf phases when the ions were started closer to the center of the trap. Also, starting the ions closer to the center increased the overall efficiency of trapping, particularly for the no-hole case, since ions were trapped over a wider range of rf phases. To understand the role of the endcap holes, a closer investigation of the ion trajectories at various rf phases is necessary.

Fig. 4 shows the trajectories of ions started 0.5 mm inside the ion trap (with and without endcap holes) at six different initial rf phases using the same conditions as in Fig. 3. For these simulations, a computational quality of 15 was used instead of the default of 2. This improved the accuracy of the numerical integration but took about five times longer to simu-

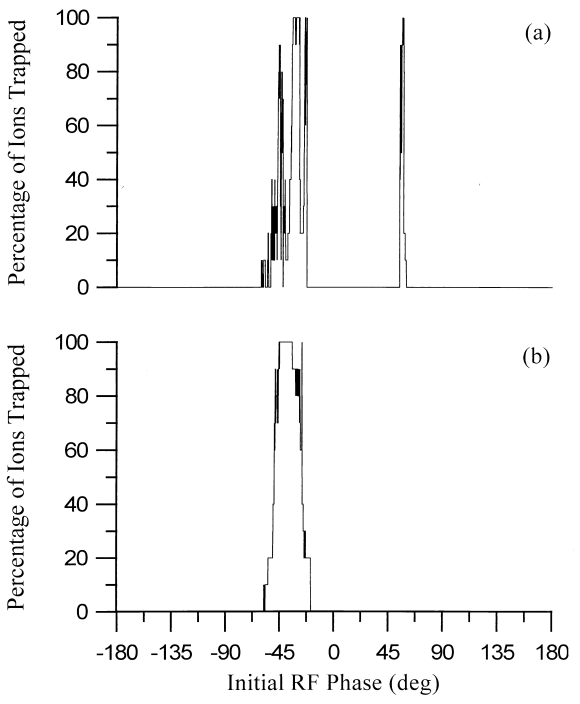

Fig. 3. Effect of endcap holes on the percentage of ions trapped as a function of initial rf phase. Same conditions as Fig. 2 except ions started 0.5 mm closer to the center of the ion trap at z_{init} = 7.35 mm. Simulation (a) with and (b) without endcap holes.

late. The axial positions of the ions are plotted versus time and the corresponding voltage applied to the ring is shown with the trajectory of each ion (see Fig. 4). Fig. 4(a) shows $\phi_{rf} = 20°$ which corresponded to the voltage on the ring starting and remaining positive at the beginning of the simulation; this caused the ions to turn around and be lost either through the endcap hole or into the endcap electrode. In Fig. 4(b), with $\phi_{rf} = 56°$, the voltage on the ring was again positive and the simulation without endcap holes showed the ion being lost to the electrode. However, with endcap holes present the ion was not lost. Equipotential contours near the endcaps indicated that the hole created a weaker rf trapping field (vide infra). This trapping field was just weak enough to prevent the ion from being repelled back out the entrance endcap hole; rather, the ion stayed in the ion trap and was successfully trapped. In Fig. 4(c), with $\phi_{rf} = 70°$, the ion is initially repelled toward the entrance endcap because the voltage on the ring electrode is positive. However, before the ion reaches the endcap (whether or not the hole is present), the voltage on the ring decreases to zero (at $\phi_{rf} = 180°$) and then becomes negative after 0.40 μs, at which time the ion is accelerated toward the center of the ion trap. As the voltage on the ring continues to oscillate between positive and negative, the ion gains sufficient axial kinetic energy to fly straight through the ion trap and strike the exit endcap or exit through the endcap hole. Fig. 4(d) shows an ion with a similar fate to that in Fig. 4(c), except the ion was started when the voltage on the ring was initially negative ($\phi_{rf} = -70°$) and therefore accelerated toward the center of the ion trap. These ions also fly straight through the ion trap and strike the exit endcap. Fig. 4(e) shows $\phi_{rf} = -30°$ where the voltage on the ring is initially slightly negative and ions are attracted toward the center of the ion trap. However, the voltage on the ring quickly swings positive and the ions are decelerated sufficiently to contain them in the ion trap and thus are trapped. Fig. 4(f) shows another discrepancy between ion trajectories with and without holes. In contrast to $\phi_{rf} = 56°$, at $\phi_{rf} = -21°$ the weak rf trapping field near the endcap hole causes the ion in the simulation with holes to be lost, while the stronger field created without holes is able to contain the ion. Although Fig. 4 only shows ion trajectories for six rf phases, the fate of ions started at all rf phases between −180° and 179° is summarized in Fig. 3.

Figs. 2 and 3 show the rf phases that result in efficient trapping of ions started at or near the endcap. However, these plots are for a specific q_z and therefore are only slices through a more complex surface mapping the percentage of ions trapped at various rf phases and q_z values. Next, both the initial rf phase and the q_z during injection were varied. The q_z was varied from 0 to 0.9 in increments of 0.005 while initial rf phase was varied from −180° to 179° in 1° increments. At each combination, ten ions were injected with different random number generator seeds for the collision model simulating a pressure of 1.5 mTorr of helium. The ions were started at the plane of the entrance endcap ($z_{init} = z_0 = 7.85$ mm) with the same initial conditions as in Fig. 2. The data are

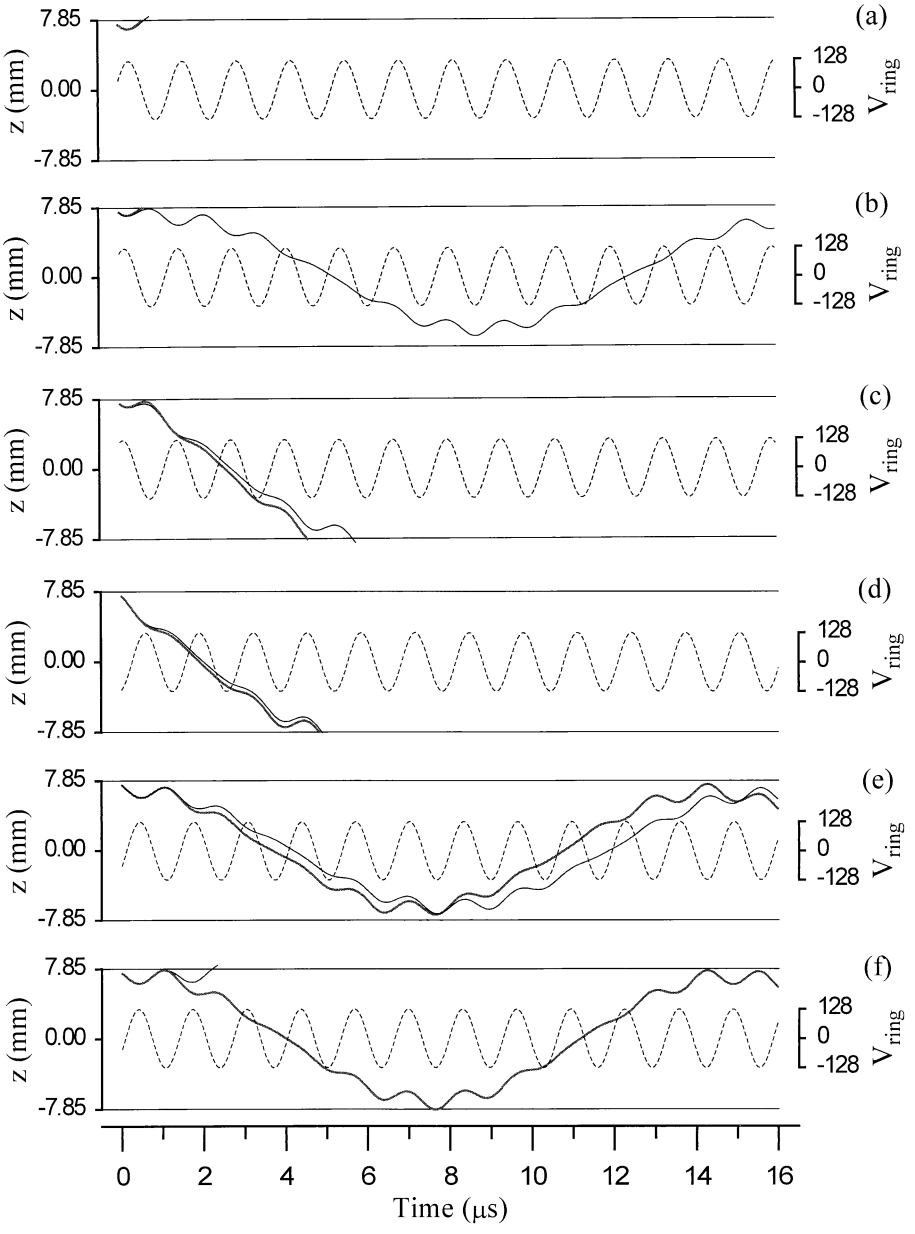

Fig. 4. Simulated trajectories of ions started 0.5 mm inside the ion trap with (thin solid line) or without (thick solid line) endcap holes for six different initial rf phases, ϕ_{rf}. Ions of m/z 100 started just inside entrance endcap ($z_{init} = 7.35$ mm, $x_{init} = 0$ mm, $y_{init} = 0$ mm) with $E_0 = 7$ eV and $\Theta = 5°$; simulated helium pressure of 1.5 mTorr; $q_z = 0.25$; $z = +7.85$ mm corresponded to the entrance endcap and $z = -7.85$ mm corresponded to the exit endcap; the corresponding voltage on the ring electrode (V_{peak}) is shown as the dotted line. (a) $\phi_{rf} = 20°$, ions are repelled toward entrance endcap. (b) $\phi_{rf} = 56°$, for the simulation with holes the ion is not lost back to the entrance endcap because of the weak rf field near the hole. (c) and (d) $\phi_{rf} = 70°$ and $-70°$, respectively, ions gain enough kinetic energy and strike the exit endcap. (e) $\phi_{rf} = -30°$, ions are trapped with or without holes. (f) $\phi_{rf} = -21°$, ions are only contained with the stronger rf field created by not having an endcap hole.

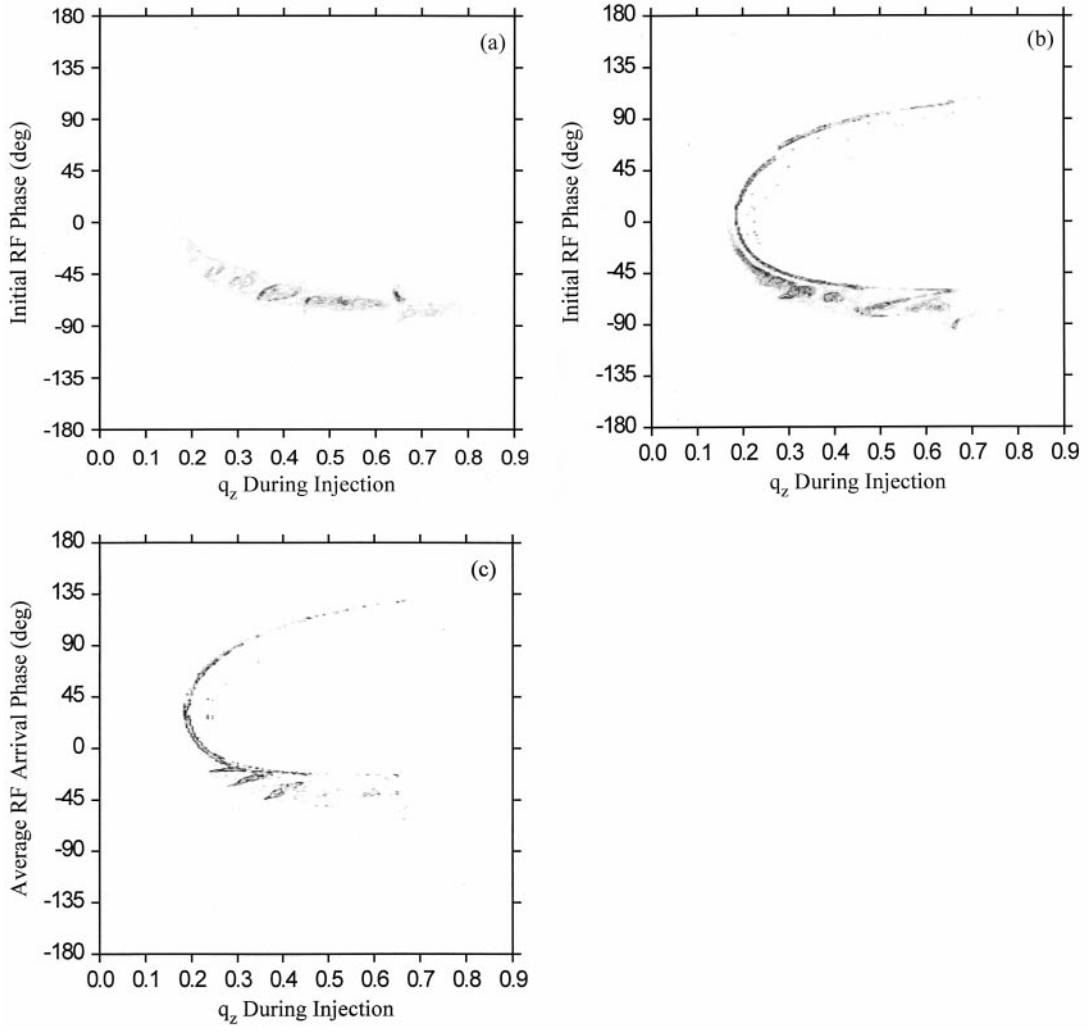

Fig. 5. Contour plots of the percentage of ions trapped as a function of rf phase and q_z for m/z 100 ions; simulated helium pressure of 1.5 mTorr. (a) No holes in endcaps and ions started at the inner plane of the entrance endcap (z_{init} = 7.85 mm, x_{init} = 0 mm, y_{init} = 0 mm, and Θ = 5°) with E_0 = 7 eV. (b) Holes in endcaps and ions started under the same conditions as in (a). Each of these simulations took over 5 days to complete. (c) Holes in endcaps and ions started outside the ion trap (z_{init} = 19 mm, x_{init} = 0.2 mm, y_{init} = 0 mm, and Θ = 0°) with E_0 = 3.5 eV (ions accelerate to 7 eV as they enter ion trap).

plotted in a series of contour plots in Fig. 5 where the z axis is the percentage of the population of ten ions which were trapped. Darker areas indicate regions where more ions were trapped. Fig. 5(a) shows that without endcap holes, there is only one range of rf phases at any q_z for which ions are efficiently trapped; however, the rf phase shifts and the width of the range of phases changes as a function of q_z. The results of including endcap holes are shown in Fig. 5(b). Here, the combinations of q_z and initial rf phase which resulted in efficient trapping showed a bullet-shaped trend. The two ranges of rf phases for which ions are trapped become closer together as the q_z during injection is lowered until they converge around q_z = 0.16, below which the rf trapping field is too weak to trap any ions.

These results indicate that the effects caused by the weakened rf field near the endcap holes are crucial to

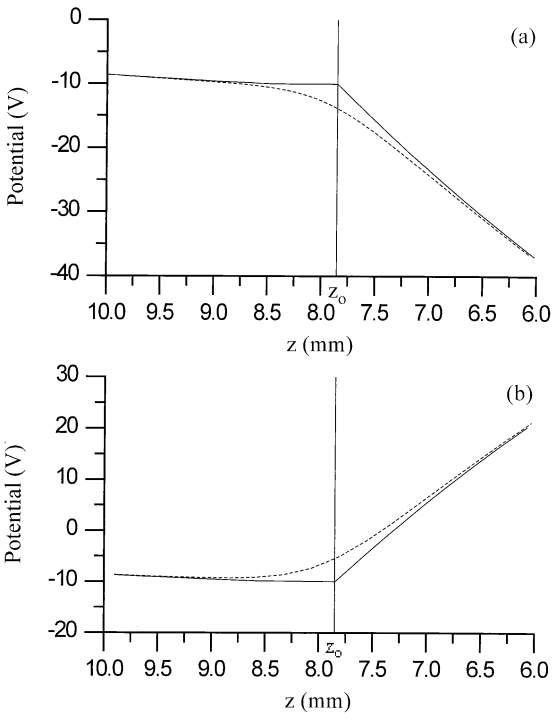

Fig. 6. Potential ions experience with (dotted line) and without (solid line) endcap holes at different z positions; $x = y = 0$ mm. (a) Ring electrode voltage is −100 V; for m/z 100 at a $q_z = 0.25$ this corresponds to a rf phase of −51°. (b) Ring electrode voltage is +95 V; for m/z 100 at a $q_z = 0.25$ this corresponds to a rf phase of 48°.

understanding injected ions. One effect the holes have is to alter the potential the ions experience near the endcap; this is shown graphically in Fig. 6. Without endcap holes, an ion started at the inner plane of the entrance endcap starts at the potential of the endcap, which in our case was −10 V. This is not the case, however, when holes are cut into the endcap electrodes. The potential in the center of the hole is not fixed, but varies as a function of the voltage on the ring electrode. With the hole in the endcap electrode, the field from the ring electrode bulges out the endcap hole (see Fig. 6). This means that the potential at the inner plane of the endcap electrode in the region of the hole will not be −10 V, the offset voltage on the ion trap. When the voltage on the ring electrode is initially negative [as in Fig. 6(a)], ions which are started at the inner plane of the endcap electrode will actually be started at a potential more negative than −10 V. Conversely, when the voltage on the ring electrode is initially positive [as in Fig. 6(b)], ions which are started at the inner plane of the endcap electrode will be started at a potential more positive than −10 V. This effect increases as the voltage on the ring is increased, since the potential at the hole will be affected to a greater extent. This field penetration out the endcap hole will cause ions started with a constant kinetic energy at the inner plane of the endcap electrode to have different starting potential energies depending on the rf phase and q_z. These different starting potentials will result in ions that travel more slowly or rapidly than they otherwise would have because of the varying amounts of acceleration the ions experience as they move toward the center of the ion trap. The most straightforward way of dealing with this problem of field penetration out the endcap holes is to start ions sufficiently far enough outside the ion trap so that the voltage on the ring does not affect the initial potential the ion experiences.

3.1.2. Ions injected from outside ion trap

Simulations were again performed in which the q_z was varied from 0 to 0.9 in increments of 0.005 and the initial rf phase from −180° to 179° in 1° increments. At each combination, ten ions were injected with different random number generator seeds for the collision model simulating a pressure of 1.5 mTorr of helium. The initial rf phases are the rf phases at which the ions were started 19 mm from the center of the ion trap. Because of their flight times to the entrance endcap electrode, the ions actually arrived at the endcap at a different rf phase. With no voltage on the ring electrode, the transit time of m/z 100 ions was 3.965 μs to the inner plane of the entrance endcap ($z = z_0$). This translates to 1084.8° of rf phase or three full rf periods plus 4.8°. The voltage applied to the ring electrode causes ions to arrive earlier or later depending on the q_z and the rf phase at which they arrive. In addition, some combinations of q_z and rf phase cause ions not to enter the ion trap at all (vide infra). Since the effect of the ring electrode voltage on the arrival phase is complex, the simulation results will simply be plotted with respect to the average rf

arrival phase defined as $(1084.8° + \phi_{rf}) - (n360°)$. In other words, the approximate transit time to the ion trap is added to the starting phase of the ion. Then, an integer number of full rf periods ($n360°$) is subtracted to make the average rf arrival phase between $-180°$ and 180°.

The results of the percentage of ions which are trapped at each q_z and average rf arrival phase are shown in Fig. 5(c). The combinations that resulted in efficient trapping showed a bullet-shaped trend similar to that seen in Fig. 5(b) for ions started at the plane of the entrance endcap; there are some important differences, however. First, the entire curve is shifted to higher phases, presumably due to field penetration out the endcap hole. Also, the bullet shape has been compressed vertically toward phases around 30°. Starting the ions at the inner plane of the entrance endcap ($z_{init} = z_0$) caused them to be started at varying potentials depending on the amount of voltage applied to the ring electrode. Starting ions at the inner plane of the entrance endcap with initial rf phases between $-180°$ and 0° means the ions are started at potentials which are more negative than they would be without the hole [see Fig. 6(a)]. The ions, therefore, undergo less acceleration than they would have if started outside the ion trap, and behave as if they are lower kinetic energy ions. As will be seen in the next set of simulations for different kinetic energy ions, a lower kinetic energy translates to ions being trapped at lower rf phases. On the other hand, starting ions with rf phases between 0° and 180° means the ions are started at more positive potentials than they would be without the hole, and therefore undergo more acceleration [see Fig. 6(b)]. These higher kinetic energy ions are trapped at higher rf phases. This distortion in the rf phases over which ions are trapped in Fig. 5(b) is eliminated by starting ions far enough outside the ion trap that field penetration out the endcap holes is insignificant [Fig. 5(c)].

3.2. Proposed model for trapping of injected ions

The question still remains as to why ions are trapped at particular q_z and rf phase combinations. Assuming an m/z 100 ion has a collision cross section of 50 Å^2, the mean free path is 41 mm with 1.5 mTorr of helium. The probability of an m/z 100 ion undergoing a collision before reaching the opposite endcap ($2z_0 = 15.7$ mm) is only about 32%. In addition, the mass difference between the m/z 100 ion and a helium atom means that only a small fraction (7.4%) of the ion's kinetic energy is lost by the ion in a single collision [see Eq. (4)]; thus, several collisions will be necessary to remove enough kinetic energy to trap the ion indefinitely. On this basis, it was speculated that ions may have trajectories at certain q_z and rf phase combinations in which the ions travel long distances in the ion trap, making possible enough collisions to remove significant kinetic energy from the ions.

In simulations, ions were injected without helium buffer gas and as expected, no ions were trapped indefinitely; indeed, 98.4% were lost within the first 20 μs. Examining the trajectories of thousands of injected ions led to the conclusion that in the absence of collisions, most ions go straight through the ion trap or turn right around and go back out the entrance endcap hole. However, there were a few q_z and rf phase combinations for which the injected ions oscillated in the ion trap for up to 622 μs without the benefit of collisional damping. These ions were termed pseudostable ions since they underwent stable trajectories for hundreds of microseconds but were not stable indefinitely. It was reasoned that these pseudostable trajectories might provide enough time for a sufficient number of collisions to occur to damp the ion's kinetic energy to a point that the ion could be trapped indefinitely. This is an extension of an idea by O and Schuessler [14] whose simulations indicated that injected ions could be stable for long enough, without the benefit of collisions, to perform spectroscopic measurements of the ions.

To test this hypothesis, simulations were performed with the q_z during injection varied from 0 to 0.9 in increments of 0.005 and the initial rf phase varied from $-180°$ to 179° in 1° increments. At each combination, a single ion was started outside the ion trap at $z_{init} = 19$ mm, $x_{init} = 0.2$ mm, and $y_{init} = 0$ mm with 3.5 eV of kinetic energy (the same conditions as for the data shown in Fig. 7) with the collision model disabled. Instead of recording whether the ions

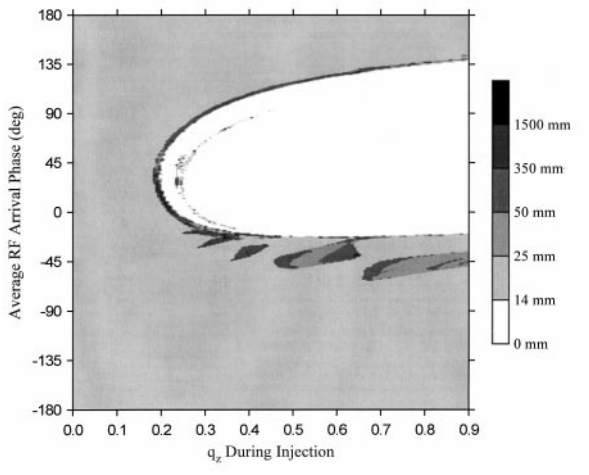

Fig. 7. Contour plot of the distance traveled by m/z 100 ions in the ion trap before being lost to an electrode or endcap hole with no helium buffer gas as a function of rf phase and q_z. Ions were started outside the ion trap (z_{init} = 19 mm, x_{init} = 0.2 mm, y_{init} = 0 mm, and Θ = 0°) with E_0 = 3.5 eV (ions accelerate to 7 eV as they enter ion trap). The q_z and rf phase combinations which resulted in naturally pseudostable trajectories are the same ones for which ions were trapped indefinitely when collisions with helium buffer gas were simulated [see Fig. 5(c)].

were trapped for >400 μs (since none of them were), the time they remained in the ion trap as well as the total distance they traveled before being lost to an electrode or endcap hole was recorded. These data are plotted in a contour plot in Fig. 7, where the z axis is the total distance traveled inside the ion trap. The white portion of the contour plot corresponds to ions which traveled less than 14 mm within the ion trap before striking an electrode or exiting through an endcap hole. These are mainly ions which turned around shortly after entering the ion trap. The lightest gray portion (14–25 mm traveled) of the plot shows ions that went straight through the ion trap and struck the exit endcap or went through the exit endcap hole. At some combinations of q_z and rf phase, the ions turned around just before striking the exit endcap and made multiple passes through the ion trap (25–1500 mm). At even fewer combinations of q_z and rf phase, the ions oscillated for even longer distances without the benefit of collisional damping (>1500 mm). Overall, the same bullet-shaped trend was observed for the longest distances traveled as was seen for the highest trapping efficiency in Fig. 5(c). The q_z and rf phase combinations for which ions "naturally" oscillated for extended periods of time (and therefore traveled large distances without collisional damping) were the same q_z and rf phase combinations for which ions were trapped indefinitely when buffer gas was added. In other words, these ions were naturally pseudostable because of the particular q_z and rf phase combination used. The ions were not stable indefinitely, but were stable long enough for sufficient collisions to occur to damp the ions and allow them to be trapped indefinitely.

The relationship between pseudostable distance traveled and the trapping of ions with helium buffer gas can be compared more closely by studying vertical slices through Figs. 5(c) and 7. Ions of m/z 100 were injected as before from outside the ion trap with E_0 = 3.5 eV and z_{init} = 19 mm from the center of the ion trap and x_{init} = 0.2 mm and y_{init} = 0 mm. Holding the q_z constant at 0.3, the initial rf phase was varied between −180° and 179.8° in 0.2° increments. The distance traveled is shown on a logarithmic scale in Fig. 8(b). The left and right sides of the curve (distances traveled around 15 mm) correspond to ions that go straight through the ion trap and are analogous to the lightest gray area in Fig. 7. rf phases with short distances traveled (<5 mm) correspond to ions which did not penetrate very deeply into the ion trap, as in the white area in Fig. 7. Between the rf phases where ions go straight through and those where the ions turn right around are rf phases where ions travel distances between 15 and 500 mm before being lost to an electrode or through an endcap hole. The percentage of ions trapped for >400 μs at a helium pressure of 1.5 mTorr is shown in Fig. 8(a). There is a strong correlation between those rf phases that resulted in naturally pseudostable trajectories and those for ions that are trapped when helium is added. Ions are only trapped at those rf phases for ion trajectories that are pseudostable for the longest distances. Increasing the helium pressure in the ion trap increases the number of collisions in a given distance and allows ions to be trapped at rf phases with shorter pseudostable distances. Simulations were performed under the same conditions as in Fig. 8(a) except the helium pressure

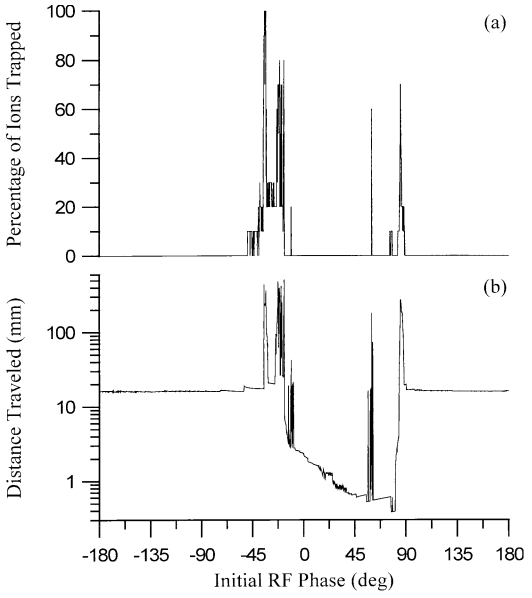

Fig. 8. Comparison of the percentage of m/z 100 ions trapped at 1.5 mTorr of helium and the distance traveled in the ion trap before being lost to an electrode or endcap hole with no helium buffer gas. Ions were started outside the ion trap (z_{init} = 19 mm, x_{init} = 0.2 mm, and y_{init} = 0 mm, and Θ = 0°) with E_0 = 3.5 eV (ions accelerate to 7 eV as they enter ion trap); q_z = 0.3. (a) Percentage of ions trapped at helium pressure of 1.5 mTorr. (b) Vertical slice from Fig. 7 showing distance traveled (on a logarithmic scale) as a function of initial rf phase; distances vary from 0.7 to 500 mm.

was varied. For helium pressures of 0.1, 1.5, 4.5, and 7.5 mTorr, the trapping efficiencies were 0.061%, 2.9%, 6.3%, and 6.4%, respectively. This increase in trapping efficiency has previously been shown in simulation [8,9] and by experiment [8].

3.3. Ion injection simulations of m/z 1522 ions

3.3.1. Effect of endcap holes on ion injection

With the insight gained from simulations of m/z 100 ions, a higher m/z ion was simulated to investigate any differences. First, the effect of endcap holes was studied. Ions were started at the inner plane of the entrance endcap electrode ($z_{init} = z_0$ = 7.85 mm, x_{init} = 0 mm, and y_{init} = 0 mm). For the following simulations, an initial kinetic energy, E_0, of 7.5 eV was used. The q_z was varied from 0 to 0.3 in increments of 0.005 and the initial rf phase was varied from −180° to 179° in 1° increments. At each combination, ten ions were injected with different random number generator seeds for the collision model simulating a pressure of 1.5 mTorr of helium; a collision cross section of 300 Å^2 was used. The data were plotted in a series of contour plots where the z axis is the percentage of the population of ten ions that were trapped. The results for the electrode grid without endcap holes are shown in Fig. 9(a), while the results with endcap holes are shown in Fig. 9(b). Just as was observed for m/z 100, without endcap holes only a single range of rf phases resulted in trapping. With endcap holes, another bullet-shaped distribution resulted. The main difference in the results compared to m/z 100 ions is that m/z 1522 ions were trapped at lower q_z values; this is consistent with experimental observations. In addition, the bullet-shaped distribution for m/z 1522 had a flatter front, meaning ions were trapped over a wider range of rf phases at low q_z values.

3.3.2. Ions injected from outside ion trap

The next step was to inject ions from outside and investigate the effect of the field distortion near the holes. Ions were started outside the ion trap at z_{init} = 19 mm, x_{init} = 0.2 mm, and y_{init} = 0 mm with 4.0 eV of kinetic energy (ions accelerate to 7.5 eV as they enter the ion trap). The q_z during injection was varied from 0 to 0.3 in increments of 0.005 and the initial rf phase was varied from −180° to 179° in 1° increments. The percentage of ions trapped with 1.5 mTorr of helium buffer gas is shown in Fig. 9(c). Instead of the anticipated bullet-shaped curve, an S-shaped curve was obtained. When ions were started at the endcap boundary, the simulations predicted efficient trapping out to $q_z \approx 0.8$ (data not shown). With ions started outside the ion trap, no ions are seen trapped above a $q_z \approx 0.2$, presumably because of the distorted field around the endcap holes.

To determine what effect the holes were having on ions, hundreds of ion trajectories were studied. These results can be summed up in the three representative trajectories shown in Fig. 10. Here, the potentials the three different ions experience as they approach the ion trap are shown as a function of time. The right

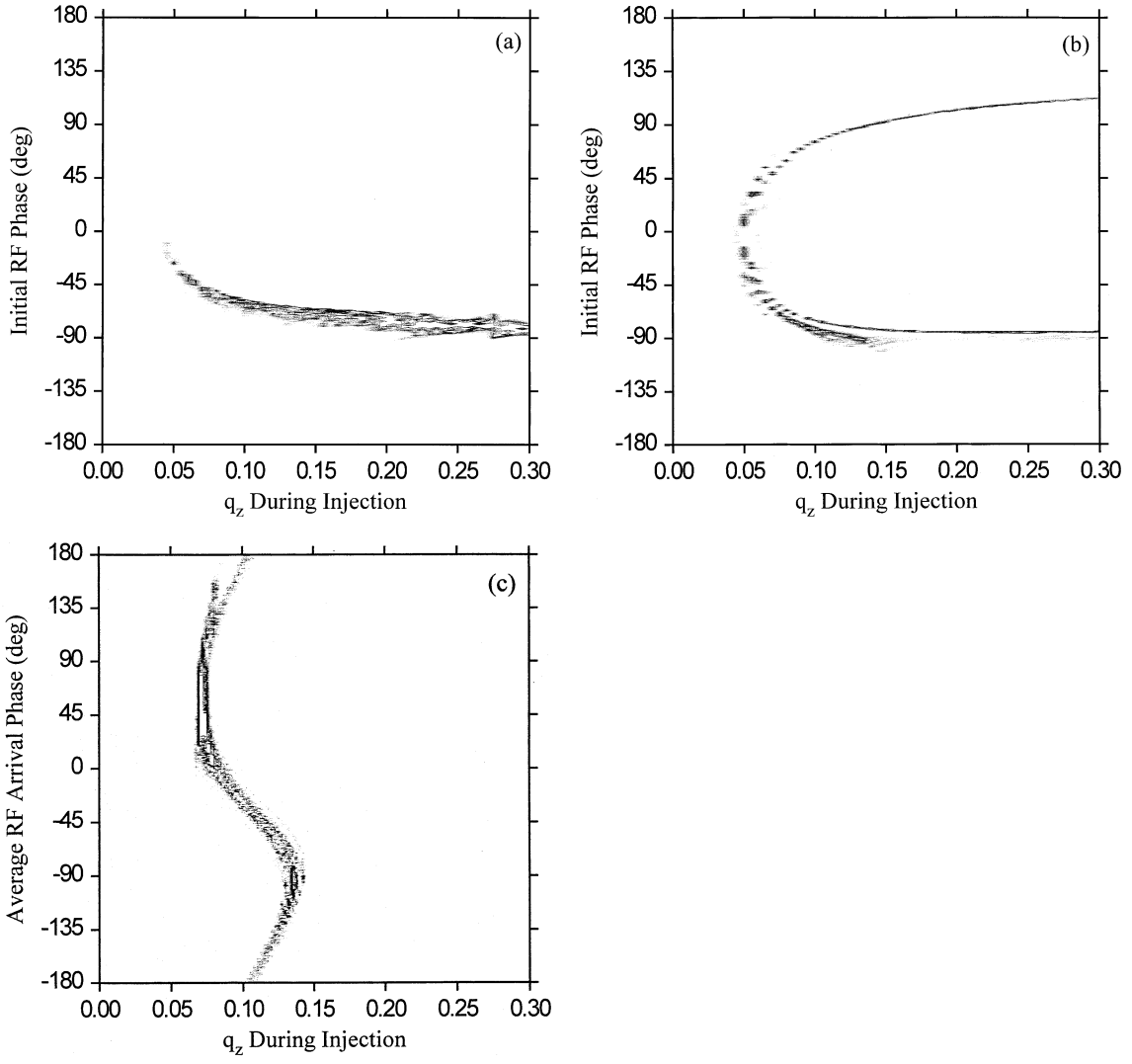

Fig. 9. Contour plots of the percentage of ions trapped as a function of rf phase and q_z for m/z 1522 ions; simulated helium pressure of 1.5 mTorr. (a) No holes in endcaps and ions started at the inner plane of the entrance endcap (z_{init} = 7.85 mm, x_{init} = 0 mm, y_{init} = 0 mm, and Θ = 10°) with E_0 = 7.5 eV. (b) Holes in endcaps and ions started under the same conditions as in (a). Each of these simulations took over 4 days to complete. (c) Holes in endcaps and ions started outside the ion trap (z_{init} = 19 mm, x_{init} = 0.2 mm, y_{init} = 0 mm, and Θ = 0°) with E_0 = 4.0 eV (ions accelerate to 7.5 eV as they enter ion trap).

edge of these plots is the time that the ions arrive at the inner plane of the entrance endcap ($z = z_0$) with no rf voltage applied to the ring electrode. All three of these ions were started under conditions such that they arrived at the entrance endcap at a rf phase of −90° in the absence of a rf voltage on the ring (shown as a dotted line). In Fig. 10(a), an m/z 100 ion was injected at a q_z of 0.6. With the rf voltage applied to the ring electrode (308 V_p), the potential outside the endcap was affected and the ion actually arrived at the endcap slightly earlier. The reason for this can be seen by returning to Fig. 6 where the rf field from the ring electrode was seen to penetrate out the endcap hole.

This effect of the rf field on the approaching ion is

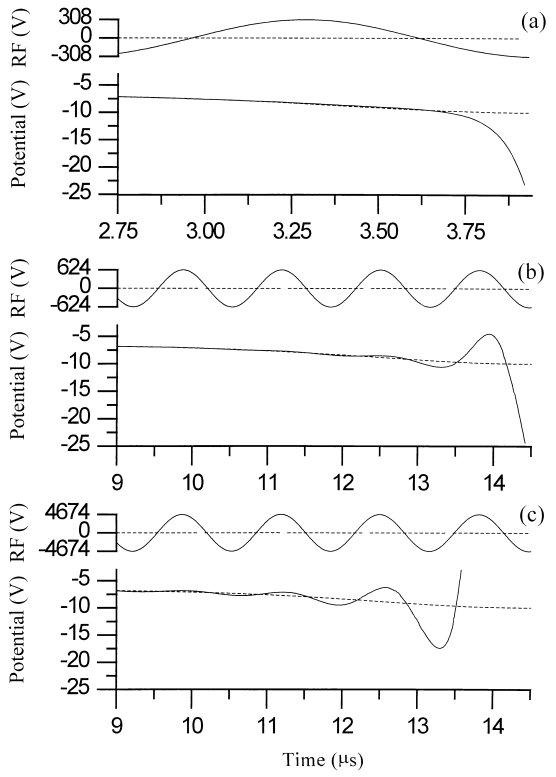

Fig. 10. Plots of the rf voltage and the potential ions experience as a function of time as they approach the ion trap from outside; the right edge of the graph is the time the ions arrive (or would have arrived in the absence of rf on the ring) at the inner plane of the entrance endcap ($z = z_0$). The dotted line is the result for no rf voltage applied to the ring electrode. (a) m/z 100 ion injected at $q_z = 0.6$. (b) m/z 1522 ion injected at $q_z = 0.08$. (c) m/z 1522 ion injected at $q_z = 0.6$; ion is repelled before it reaches the ion trap.

even more dramatic for an m/z 1522 ion injected at a $q_z = 0.08$, as shown in Fig. 10(b). Here, the rf field which penetrates out the endcap was even stronger because the rf voltage on the ring electrode was approximately twice as high (624 V_p) as in Fig. 10(a). More importantly, the m/z 1522 ion was moving more slowly than the m/z 100 ion; therefore, the m/z 1522 ion interacted with more rf periods than the m/z 100 ion. Although the m/z 1522 ion should have arrived at the ion trap at a rf phase of $-90°$, it interacted strongly with a positive phase of the rf voltage when the ion was approximately 0.55 mm outside the ion trap. This interaction presented the ion with a potential hill, which fortunately, the ion was able to climb. The only side effect was the ion arrived at the endcap slightly later than it would have if it were not for this rf field penetration. This potential hill got larger when the rf voltage on the ring electrode was increased (higher q_z). Fig. 10(c) shows the case for a q_z of 0.6, where the ion was affected by the rf voltage on the ring electrode as far as 4.5 mm from the entrance endcap. This interaction was so strong that an insurmountable potential hill repelled the ion when it was 0.6 mm from the inner boundary of the endcap. Although ions can be trapped at high q_z [as shown in Fig. 9(b)], this rf field penetration prevents them from ever entering the ion trap. A similar effect was reported in the literature where the authors mentioned that some of their computer simulations showed that ions which arrived at the wrong rf phases could be forced back into the endcap hole and therefore never get into the ion trap [5]. Although the authors were correct, they did not appreciate that ions could actually be repelled long before they even reach the ion trap. Furthermore, even if the rf field penetration was not strong enough to repel the ions, it could cause the ions to arrive earlier or later than they otherwise would have. These effects cause the bullet-shaped curve [Fig. 9(b)] to open up to an S-shaped curve (Fig. 10).

3.4. Comparison of ion injection experiments to computer simulations

These SIMION computer simulations have provided significant insight into how injected ions are trapped. Moreover, the SIMION model has raised several questions about the effect of endcap holes and rf field penetration. Although these effects make sense, they have not been reported in the literature and cannot be easily measured experimentally. What has been measured experimentally is the relative trapping efficiency as a function of q_z during injection. The ability of the simulations to predict these experimental observations would help validate the model and many of its other predictions.

Since electrospray is a continuous ionization source, the percentage of the ions successfully trapped

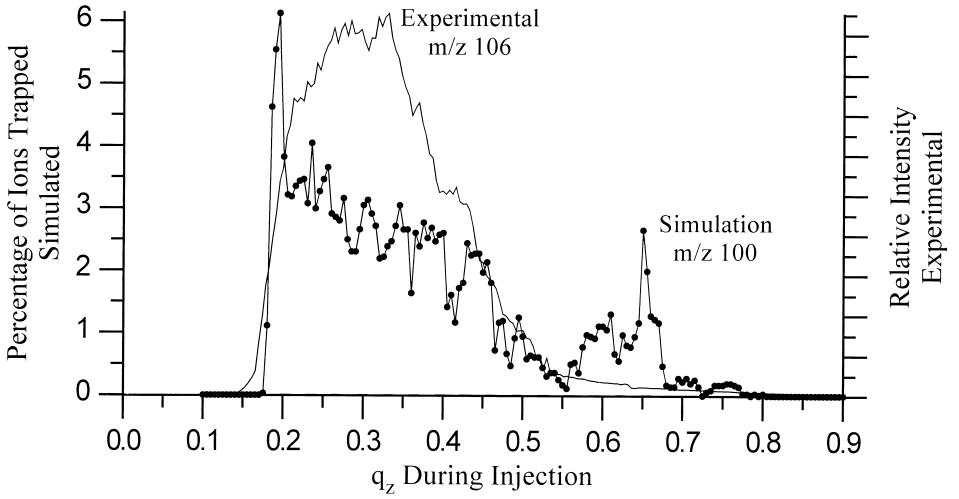

Fig. 11. Comparison of simulation of m/z 100 and experimental ion injection data for m/z 106.1. Simulated data show the percentage of ions trapped at each q_z (out of 3600) over all rf phases for a single kinetic energy of 7 eV.

at each q_z can be calculated by summing the number of ions trapped over all initial rf phases and dividing by the total number of ions injected at that q_z. The percentage of m/z 100 ions trapped at each q_z in Fig. 5(c) was calculated and is plotted in Fig. 11. Also, the experimental variation of m/z 106.1 is shown in Fig. 11 for comparison. Overall, the results do not agree very strongly; the simulated data show a sharp spike of high injection efficiency at the left edge near $q_z = 0.2$ and a gradual drop in efficiency at higher q_z. In contrast, the experimental data show a sloping left edge between $q_z = 0.15$ and 0.2 and a broader optimum. In the simulation, there was an interesting increase in trapping efficiency around a q_z of 0.65; the inability to trap m/z 106.1 ions at higher q_z values presumably results from fragmentation of the ions (vide infra). Similar increases in trapping efficiency near $q_z = 0.65$ have been previously reported [39–41]. Although the exact cause of the increase is unknown, it is suspected to be related to the octopolar nonlinear resonance at $\beta_z = 1/2$ [39].

One reason for the inconsistency between simulation and experiment was the simulation used ions of only a single kinetic energy, 7 eV. This kinetic energy was chosen because it was the center of the energy distribution as measured by experimental stopping potentials for m/z 106.1. However, the derivative of the stopping potential data also provided the kinetic energy distribution of the ion beam. The kinetic energy distribution was centered at 7 eV; however, it had a full width at half maximum (FWHM) kinetic energy spread of approximately 2.5 eV. This relatively broad kinetic energy distribution was caused by collisions in the first octopole [31] which contained approximately 2 mTorr of nitrogen. To determine the effect of kinetic energy on ion injection, simulations such as those summarized in Fig. 5(c) were repeated for ions with initial kinetic energies of 1.5, 2.5, 4.5, and 5.5 eV to simulate ions entering the ion trap with 5, 6, 8, and 9 eV kinetic energies. From these data, the left edge of the bullet-shaped curve in Fig. 5(c) was found to shift to higher q_z at higher injection kinetic energies. This is consistent with the experimental observation that higher kinetic energy ions are more efficiently trapped at higher q_z values [2]. Also, as the kinetic energy was increased, the bullet-shaped curve became narrower in phase, resulting in a shift in the advantageous rf phases toward the center of the bullet.

Since ions of different initial kinetic energies travel at different velocities, the transit time to the entrance endcap is different. To allow all five kinetic energy simulation plots to be shown together, the initial rf phases were converted to the average rf arrival phase, as in Fig. 5(c). Next, the number of ions trapped at

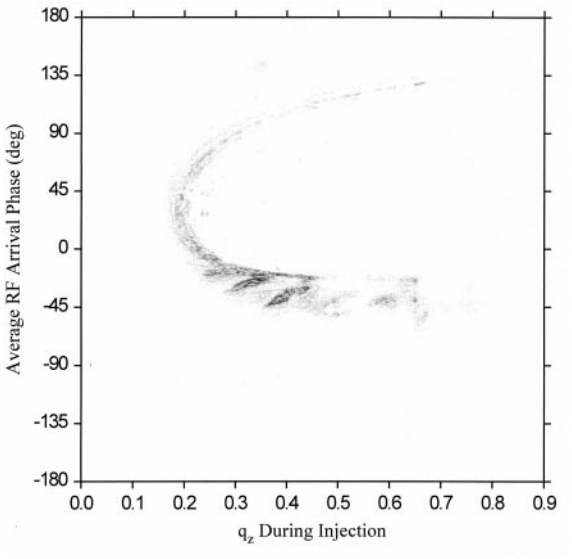

Fig. 12. Contour plot of the percentage of ions trapped as a function of average rf arrival phase and q_z, compiling simulations of m/z 100 ions injected at 5, 6, 7, 8, and 9 eV. The simulations of multiple kinetic energies were weight-summed according to the percentage of each kinetic energy found in the experimental ion beam for m/z 106.1. Lower kinetic energy ions are trapped at lower q_z values. Initial rf phase was converted to average rf arrival phase to allow all five simulations to be compared on the same plot. Ions were started outside the ion trap (z_{init} = 19 mm, x_{init} = 0.2 mm, y_{init} = 0 mm, and $\Theta = 0°$). Simulated helium pressure of 1.5 mTorr.

each kinetic energy was scaled based on the percentage of ions in the experimental ion beam with that kinetic energy (data not shown). A contour plot summarizing all five kinetic energies between 5 and 9 eV is shown in Fig. 12. The effect of the weighted summing of a range of kinetic energies is to broaden the range of q_z values and rf phases over which ions are trapped, as can be observed by comparing Figs. 12 and 5(c). The percentage of ions trapped over all rf phases was then calculated for each q_z as in Fig. 11. This new simulated profile for m/z 100 is shown in Fig. 13 along with the experimental data for m/z 106.1.

Overall, the agreement between the simulation and experimental data is quite good at q_z values below 0.55. The weighted summing of multiple kinetic energies has the effect of broadening the range of q_z values over which ions are trapped so that a broader optimum results as seen experimentally. At q_z values above 0.55, a possible explanation for the discrepancy between the experimental and simulated data shown in Fig. 13 is ion fragmentation. It has been observed experimentally that the ion signal of injected ions drops off at high q_z during injection, primarily because the injected ions fragment [2,12,42]. At high q_z values for injection, fragment ions of m/z 106.1 were

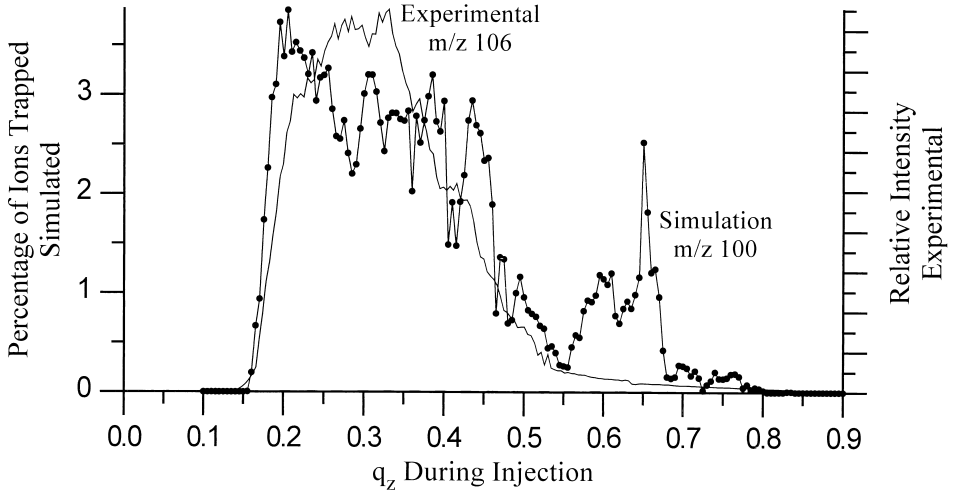

Fig. 13. Comparison of simulation of m/z 100 and experimental ion injection data for m/z 106.1. Simulated data show the percentage of ions trapped at each q_z (out of 18 000) over all rf phases weighted for an experimentally determined range of kinetic energies (5–9 eV).

observed in the spectra for the data shown in Fig. 13. According to pseudopotential well theory, the average kinetic energy of an ion is proportional to q_z^2; therefore, at higher q_z values ions undergo more energetic collisions [27]. Also, at higher kinetic energy the ions are moving faster and travel more distance per unit time; therefore, they undergo more collisions per unit time. Since the hard-sphere collision model in the simulation does not take into account internal energy deposition or fragmentation, the simulation may predict trapping at q_z values for which experimental ions fragment. It would be interesting to incorporate fragmentation into future computer simulation studies.

In addition to modeling the ion injection trends seen experimentally, the simulation also provides absolute percentages of ions trapped at each q_z, which is quite challenging to measure experimentally. The maximum percentage of m/z 100 ions trapped was found to be around 3% for q_z values between 0.2 and 0.4. This trapping efficiency is consistent with what has been measured experimentally [10,12]. It should be noted that the data shown in Figs. 12 and 13 consisted of simulations of (3600 ions/energy/q_z) $\times$ (5 energies) or 18 000 total ions at each q_z. With the 181 q_z values simulated, these plots comprised 3 258 000 ions and required 28 days to simulate.

This same type of analysis was performed for m/z 1522. From experimental stopping potential measurements, m/z 1522 ions were found to have an average kinetic energy of 7.5 eV and a 2.5 eV FWHM distribution of kinetic energies (data not shown). Additional simulations were run with initial kinetic energies of 2, 3, 5, and 6 eV to simulate ions entering the ion trap with 5.5, 6.5, 8.5, and 9.5 eV. The percentage of ions trapped at each kinetic energy was weighted based on the experimental stopping potential distribution; the resulting contour plot is shown in Fig. 14. The left edge of the S-shaped curve was found to shift to higher q_z at higher injection kinetic energies. Also, as the kinetic energy was increased, the S-shaped curve flattened out, narrowing the range of efficient q_z values. At the same time, ions were trapped over a wider range of rf phases than for the higher velocity, lower m/z 100 ion.

The percentage of the ions successfully trapped at each q_z was calculated by summing the number of ions trapped over all initial rf phases and dividing by the total number of ions injected at that q_z. The percentage of m/z 1522 ions trapped is plotted as a function of q_z during injection in Fig. 15 and shown in comparison to the experimental variation of m/z 1522. The simulations do not predict as wide a range of q_z values for efficient trapping as observed experimentally. This and the humps observed in the tail of the simulation data may be a result of the discrete kinetic energies used as well as the simulation of only a single initial position. More simulations may improve the agreement between simulation and experiment; however, the data shown already represent the combined simulations of 1 098 000 ions and took 20 days to simulate. Despite these differences, it is important to note that the m/z 1522 ions were trapped over a narrower range of q_z values and centered at a

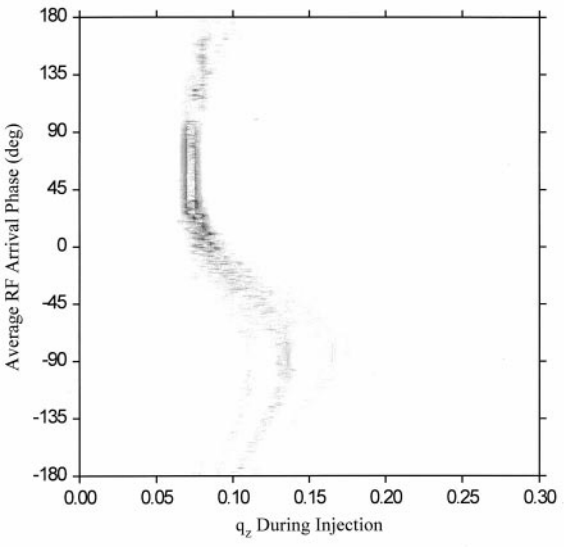

Fig. 14. Contour plot of the percentage of ions trapped as a function of average rf arrival phase and q_z compiling simulations of m/z 1522 ions injected at 5.5, 6.5, 7.5, 8.5, and 9.5 eV. The simulations of multiple kinetic energies were weight summed according to the percentage of each kinetic energy found in the experimental ion beam for m/z 1522. Lower kinetic energy ions are trapped at lower q_z values. Initial rf phase was converted to average rf arrival phase to allow all five simulations to be compared on the same plot. Ions were started outside the ion trap (z_{init} = 19 mm, x_{init} = 0.2 mm, y_{init} = 0 mm, and Θ = 0°). Simulated helium pressure of 1.5 mTorr.

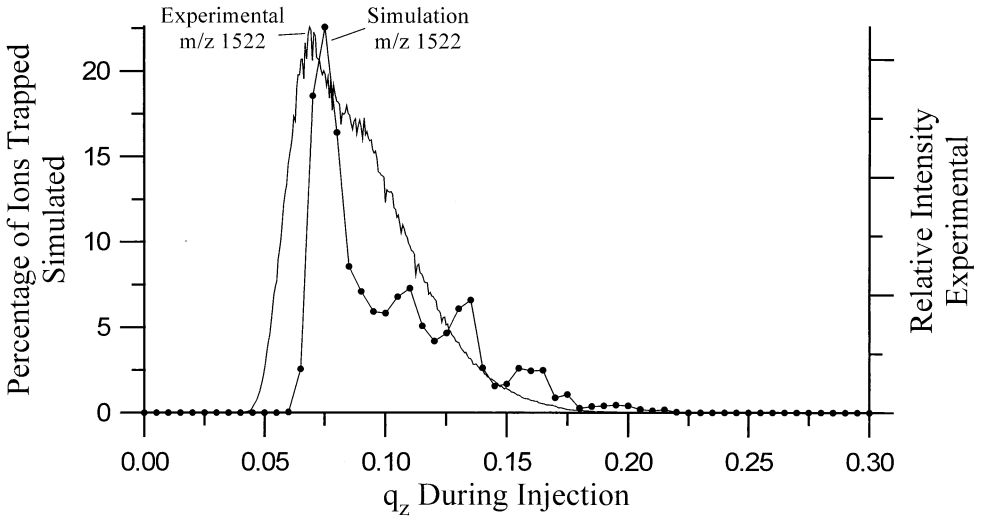

Fig. 15. Comparison of simulation of m/z 1522 and experimental ion injection data for m/z 1522. Simulated data show the percentage of ions trapped at each q_z (out of 18 000) over all rf phases for an experimentally determined range of kinetic energies (5.5–9.5 eV).

lower q_z than the m/z 100 ions. The optimum q_z for trapping was ≈0.3 for m/z 100 and ≈0.075 for m/z 1522. This corresponds to a rf voltage of 154 V_p for m/z 100 and 584 V_p for m/z 1522. The more slowly moving m/z 1522 ion is affected to a greater extent than the m/z 100 ion by rf field penetration as it approaches the trap because of the larger rf voltages on the ring electrode, as shown in Fig. 10. This rf field penetration is beneficial in this case because a higher percentage of ions are trapped than for m/z 100; in fact, the maximum trapping efficiency was 22.6% for m/z 1522 (Fig. 15) versus 3.9% for m/z 100 (Fig. 13).

Although the agreement between the simulated and experimental data was quite good, the question remains as to how important it is in simulations to start ions outside the ion trap. Recall that the rf fringe field dramatically changed the shape of the rf phase and q_z contour plot for ions started outside the ion trap [compare Fig. 9(b) to Fig. 9(c)]. The main discrepancy is that simulations starting ions at the endcap predicted trapping well beyond a q_z of 0.2, where experimentally no ions were observed. Although it is tempting to explain this with the same ion fragmentation at high q_z argument used above, no fragmentation was observed experimentally. The hypothesis is that although ions can be trapped at these higher q_z values, the rf fringe field prevents ions from entering the ion trap in the first place, as shown in Fig. 10. rf field penetration out of the endcap hole suggests that simulation programs which only model the field within the ion trap (forcing ions to be started at the endcap boundary) are not adequate for simulating ion injection.

4. Conclusions

Ion injection into a quadrupole ion trap mass spectrometer was studied by both simulation and experiment. SIMION was chosen because it allowed the actual electrode geometry including endcap holes to be simulated. The endcap holes weaken the rf trapping field in the region near the holes; this distortion of the field is important when ions have large axial trajectories as they do in ion injection. All previous simulations of ion injection have predicted a single, narrow range of rf phases when the voltage on the ring electrode is initially negative for which injected ions are successfully trapped. However, the inclusion of the endcap holes created a weakened rf trapping field near the holes which allowed ions to be

trapped over a second narrow range of rf phases when the ring is initially positive.

A model for the process by which injected ions are trapped was developed using the SIMION simulations. Injected ions can be trapped even with the modest helium buffer gas pressures commonly used in ion traps (≈1 mTorr) because ions naturally oscillate for long times (and therefore distances) at certain q_z and initial rf phases. This allows enough collisions to occur to damp the ions' excess kinetic energy. However, the small range of favorable rf phases and the inefficiency of collisional damping demands further study to maximize the number of ions which are trapped.

In simulations performed where ions were started outside the ion trap, the results agreed well with experimental ion injection data for both m/z 100 and 1522 ions. It was necessary to start ions outside the ion trap because field penetration of the rf field out the endcap hole affected ions as they approached the ion trap. This field penetration had a larger influence on the more slowly moving m/z 1522 ions compared to m/z 100 ions of similar kinetic energy. As the ions approached the ion trap, the rf field penetrating out of the endcap hole affected the phase at which the ions entered the ion trap by slowing down and speeding up the ions as they approached the entrance endcap.

Acknowledgements

S.T.Q. would like to acknowledge a NASA Space Grant Fellowship supported through the Florida Space Grant Consortium and Finnigan MAT, as well as an ACS Analytical Division Fellowship supported by Eli Lilly. Also, S.T.Q. would like to thank Jae C. Schwartz and John E. P. Syka for many helpful discussions.

References

[1] W. Paul, H. Steinwedel, U.S. Patent No. 2939952 (1960).
[2] J.N. Louris, J. Amy, T. Ridley, R.G. Cooks, Int. J. Mass Spectrom. Ion Processes 88 (1989) 97–111.
[3] S.A. McLuckey, G.J. vanBerkel, D.E. Goeringer, G.L. Glish, Anal. Chem. 66 (1994) 689A–696A.
[4] R.E. March, J.F.J. Todd, Practical Aspects of Ion Trap Mass Spectrometry, CRC, New York, 1995.
[5] R.B. Moore, S. Gulick, Phys. Scripta T22 (1988) 28–35.
[6] V.M. Doroshenko, R.J. Cotter, Rapid Commun. Mass Spectrom. 7 (1993) 822–827.
[7] G.C. Eiden, A.W. Garrett, M.E. Cisper, N.S. Nogar, P.H. Hemberger, Int. J. Mass Spectrom. Ion Processes 136 (1994) 119–141.
[8] Y. Wang, M. Schubert, J. Franzen, Proceedings of the 43rd ASMS Conference on Mass Spectrometry and Allied Topics, Atlanta, GA, 1995, p. 1106.
[9] C. Weil, M. Nappi, C.D. Cleven, H. Wollnik, R.G. Cooks, Rapid Commun. Mass Spectrom. 10 (1996) 742–750.
[10] J. Qin, B.T. Chait, Anal. Chem. 68 (1996) 2102–2107.
[11] E. Fischer, Z. Phys. 156 (1959) 1–26.
[12] S.A. McLuckey, G.L. Glish, K.G. Asano, Anal. Chim. Acta 225 (1989) 25–35.
[13] P.H. Dawson, C. Lambert, Int. J. Mass Spectrom. Ion Processes 16 (1975) 269–280.
[14] C.S. O, H.A. Schuessler, J. Appl. Phys. 52 (1981) 1157–1166.
[15] J.E.P. Syka, in Practical Aspects of Ion Trap Mass Spectrometry Vol. I Fundamentals of Ion Trap Mass Spectrometry, R.E. March, J.F.J. Todd (Eds.), CRC, New York, 1995, pp. 169–205.
[16] J.N. Louris, J.C. Schwartz, G.C. Stafford, J.E.P. Syka, D.M. Taylor, Proceedings of the 40th ASMS Conference on Mass Spectrometry and Allied Topics, Washington, DC, 1992, pp. 1003–1004.
[17] J. Franzen, R.H. Gabling, G. Heinen, G. Weiß, Proceedings of the 38th ASMS Conference on Mass Spectrometry and Allied Topics, Tucson, AZ, 1990, pp. 417–418.
[18] M.D.N. Lunney, J.P. Webb, R.B. Moore, J. Appl. Phys. 65 (1989) 2883–2888.
[19] J. Franzen, R.H. Gabling, M. Schubert, Y. Wang, in Practical Aspects of Ion Trap Mass Spectrometry, Vol. I: Fundamentals of Ion Trap Mass Spectrometry, R.E. March, J.F.J. Todd (Eds.), CRC, New York, 1995, pp. 49–167.
[20] J. Franzen, Int. J. Mass Spectrom. Ion Processes 106 (1991) 63–78.
[21] F.A. Londry, R.L. Alfred, R.E. March, J. Am. Soc. Mass Spectrom 4 (1993) 687–705.
[22] R.E. March, F.A. Londry, R.L. Alfred, J.F.J. Todd, A.D. Penman, F. Vedel, M. Vedel, Int. J. Mass Spectrom. Ion Processes 110 (1991) 159–178.
[23] H.P. Reiser, R.K. Julian, R.G. Cooks, Int. J. Mass Spectrom. Ion Processes 121 (1992) 49–63.
[24] R.K. Julian, H.P. Reiser, R.G. Cooks, Int. J. Mass Spectrom. Ion Processes 123 (1993) 85–96.
[25] R.K. Julian, M. Nappi, C. Weil, R.G. Cooks, J. Am. Soc. Mass Spectrom. 6 (1995) 57–70.
[26] H.J. Kluge, G. Bollen, Hyp. Int. 81 (1993) 15–26.
[27] R.E. March, H.E. Hughes, Quadrupole Storage Mass Spectrometry, Wiley, New York, 1989.
[28] R.D. Knight, Int. J. Mass Spectrom. Ion Processes 51 (1983) 127–131.
[29] J.C. Schwartz, M.E. Bier, D.M. Taylor, J. Zhou, J.E.P. Syka,

M. James, G.C. Stafford, Proceedings of the 43rd ASMS Conference on Mass Spectrometry and Allied Topics, Atlanta, GA, 1995, p. 1114.
[30] D.J. Douglas, J.B. French, J. Am. Soc. Mass Spectrom. 3 (1992) 398–408.
[31] T. Covey, D.J. Douglas, J. Am. Soc. Mass Spectrom. 4 (1993) 616–623.
[32] M.W.E.M. vanTilborg, J. vanThuijl, Org. Mass Spectrom. 19 (1984) 217–220.
[33] J.J. vanHoute, C.G. deKoster, J. vanThuijl, J. Int. J. Mass Spectrom. Ion Processes 115 (1992) 173–183.
[34] S.G. Roussis, J. Am. Soc. Mass Spectrom. 6 (1995) 803–811.
[35] C.S. O, H.A. Schuessler, J. Phys. D: Appl. Phys. 14 (1981) 953–960.
[36] H.A. Schuessler, C.S. O, Nucl. Instr. Methods 186 (1981) 219–230.
[37] C.S. O, H.A. Schuessler, J. Appl. Phys. 52 (1981) 2601–2607.
[38] C.S. O, H.A. Schuessler, Int. J. Mass Spectrom. Ion Processes 40 (1981) 53–66.
[39] R.E. Pedder, R.A. Yost, M. Weber-Grabau, Proceedings of the 37th ASMS Conference on Mass Spectrometry and Allied Topics, Miami Beach, FL, 1989, pp. 468–469.
[40] J.D. Williams, H.P. Reiser, R.E. Kaiser, R.G. Cooks, R.G. Int. J. Mass Spectrom. Ion Processes 108 (1991) 199–219.
[41] S.M. Boué, J.A. Jones, R.A. Yost, Proceedings of the 42nd ASMS Conference on Mass Spectrometry and Allied Topics, Chicago, IL, 1994, p. 218.
[42] J.C. Schwartz, R.G. Cooks, M. Weber-Grabau, P.E. Kelley, Proceedings of the 36th ASMS Conference on Mass Spectrometry and Allied Topics, San Francisco, CA, 1988, pp. 634–635.